A NEW METHODOLOGY FOR ENGINE INSTALLATION EFFECT PREDICTION USING MACHINE LEARNING

DI MARCO Alexandre
Engine performance engineer
Airbus Helicopters
Marignane, France

ESTERLE Florent
Engine performance engineer
Airbus Helicopters
Marignane, France

GAULMIN François-Xavier
Technical auditor & executive
Expert powerplant
Airbus Helicopters
Marignane, France

Abstract

This paper presents a machine learning approach to predict the effects of installing new air intake system, thus reducing the need for extensive flight tests. The following method is used: firstly, a machine learning model is used to predict the characteristics of the flow entering the engine; secondly, an engine thermodynamic model is used to predict the engine's response to disturbance. Several models were evaluated, and the gradient boosting model proved to be the most promising, with very good R^2 scores and low MAEs to introduce an error as low as possible in the evaluation of installation effects. Validation by comparison with real flight tests shows that the model is able to accurately predict the aerodynamic characteristics entering the engine. Finally, this model is applied to a real case study and the installation effects computed with the method explained in this paper are used and show a very good prediction of the installation effects with less than 1% absolute error on the prediction. This methodology offers a new way of reducing air intake development costs and improving overall performance by reliably estimating installation effects.

NOTATION

Symbols

N_1	Corrected gas generator speed
ITT	Inter-Turbine Temperature
Pu	Power [kW]
PI	Installation losses [%]
SFC	Specific Fuel Consumption [kg/kWh]
ΔP	Pressure drop [%]
ΔT	Temperature rise [K]
DC_{60}	Pressure distortion index
$P_{t60^\circ,\min}$	Minimal pressure on a sector of 60°
$P_{t,\text{mean}}$	Mean Total pressure
TC_{120}	Temperature distortion index
$T_{t120^\circ,\max}$	Maximal temperature on a sector of 120°
$T_{t,\text{mean}}$	Mean total temperature
R^2	Coefficient of Determination

Acronyms

MAE	Mean Absolute Error
CFD	Computational Fluid Dynamics
MLP	Multi-Layer Perceptron
SVR	Support Vector Regression
AIP	Aerodynamic Interface Plane
KNN	K-Nearest Neighbors

1 INTRODUCTION

The efficiency and performance of helicopters are greatly enhanced by the integration of turboshaft engines, recognized for their excellent power-to-weight ratio. However, integrating these engines within the airframe, i.e. interfacing with air intake and exhaust systems, introduces aerothermal and aerodynamic disturbances known as contributors to installation effects. These disturbances can lead to power losses and increased fuel consumption, impacting the overall performance and operability Ref. 1.

In this context, many flight tests are conducted to ensure accurate characterization of engine performance. These tests typically include:

- Flight tests to ensure good quality air flow to the engine, minimizing pressure drops, pressure distortions, temperature rise, and temperature distortions. These verifications are normally carried out during all flight phases using special instruments (e.g., pressure/temperature sensors at AIP) to demonstrate that the aircraft's air intake conditions meet the engine manufacturer's compressor inlet requirements, ensuring there is no risk of engine surge.

- Flight tests to determine installation effects from various sources, with air intake being the main contributor. These tests can be numerous (and thus expensive) due to the number of flight conditions that must be met to accurately determine the installation effect (altitude, temperature, power level, speed, climb, etc.), resulting in scattered results requiring an extensive test campaign.

In some cases, the same helicopter with the same engine may require different air intake configurations (e.g., filtered air intake as an alternative to non-filtered), offering helicopter customers multiple options depending on their usage. In such scenarios, the above test types must be repeated for each air intake configuration.

Currently, the conventional method for assessing installation effects involves characterizing the engine performance on a test bench to evaluate its performance throughout the flight envelope. The same engine is then installed on the helicopter, and dedicated flight tests are performed to determine the installation effect as the difference between the engine power measured in flight and on the test bench. Although this method quantifies installation effects, achieving a deterministic understanding remains challenging. There is often considerable scatter in the results, making it difficult to achieve good accuracy to ensure maximum helicopter performance.

Previous work in Ref. 2 proposed a physical approach to predicting installation effects to reduce development risk and cost. This method uses CFD simulations to determine the aerodynamic and aerothermal disturbances created by the helicopter air intake, and a thermodynamic engine model to estimate installation effects. Although this method provides good preliminary estimations, but it has limitations such as imprecise predictions at a given ITT and an inability to capture scattering. Di Marco et al. Ref. 3 addressed some ITT inaccuracies but still failed to assess the scattering. They suggest that scattering is probably due to parameters not accounted for in CFD, such as the homogeneity of the air intake flow conditions Ref. 4, which is affected by the aircraft's attitude. Variations in swirl patterns observed in the intake, as shown in Ref. 5, are linked to pressure distortion, implying that the aircraft's attitude affects aerodynamic criteria, particularly pressure distortion, introducing scattering in flight test results. However, performing CFD calculations for all scenarios would be highly resource consuming (CPU, time, ...).

To address these challenges, machine learning techniques have become powerful tools in aerospace engineering Ref. 6. They offer significant potential for developing surrogate models that can predict complex patterns with high accuracy. Various machine learning models, including neural networks, support vector machines, and ensemble methods, are able to learn non-linear relationships from data, making them particularly well-suited for modeling engine behavior Ref. 7, aircraft performance Ref. 8, aerodynamics Ref. 9, and more. Recent studies highlight the transformative potential of machine learning across various aeronautical applications, including performance prediction, fault detection, and optimization. Machine learning-based surrogate models can deliver high-fidelity predictions while significantly reducing the computational cost compared to traditional CFD simulations Ref. 10.

To overcome these limitations, this paper proposes a new approach based on machine learning methods. The goal is to determine if machine learning can help minimize the need of flight tests to perform, especially by avoiding the extensive installation effects testing campaign for another air intake configuration. This approach uses:

- The complete results from an initial testing campaign dedicated to a first air intake configuration.
- The results from a limited testing campaign that verifies the engine's air supply conditions.

The proposed method involves creating a surrogate model to determine aerodynamic and aerothermal disturbances, called system loss, which is generated by the new air intake system using dedicated flight tests to ensure engine airflow quality. This system loss is then combined with a thermodynamic engine model to determine installation effects from available flight data for the original air intake, thus removing the need for dedicated flight test. This paper describes the methodology, evaluating different machine learning models for the best results. The hyperparameters and accuracy of the model are analyzed, and the method is assessed by comparing the expected installation effects of the intake barrier filter (IBF) with the installation effects measured during flight tests.

In summary, this paper proposes a new machine learning-based approach for predicting installation effects. The goal is to achieve the same accuracy as the current method of determining installation effects, while reducing the need for expensive flight tests. Using the ability of machine learning algorithms to learn complex patterns and relationships, this approach can provide a new way to evaluate facility effects, allowing a helicopter manufacturer to reduce the number of flight tests.

2 METHOD

2.1 Installation effect definition

Air intake Installation effect on engine is the key concept behind the assessment of the engine performance installed on an helicopter and thus particular attention shall be made for its modelisation.

Installation effects are defined as the difference between the power delivered by the engine on the bench and the power delivered by the engine once installed on the helicopter, when an engine limit is encountered, and the fuel flow variation for a given power. Today, installation effects are established as follows: The engine is characterized on an engine manufacturer's test bench to assess its performance throughout the flight envelope. The same engine is then installed in a helicopter, and its performance are measured during dedicated flight tests. The difference in power and fuel flow between the helicopter flight and the test bed are the installation effect. Figure 1 explains how installation effects are defined.

Therefore, according to the definition, the installation effects in terms of power are perceivable only when the engine is limited. If an engine limit is not reached, the engine will therefore increase the fuel flow to reach the required power level. An additional installation effect is defined, this time with a fixed power level, and in this case, to compare the impact of the installation on the specific consumption of the engine. The installation effects are defined by the following two equations:

$$PI(\%) = \frac{Pu_{Installed} - Pu_{Uninstalled}}{Pu_{Uninstalled}} \tag{1}$$

$$PI_{SFC}(\%) = \frac{SFC_{Installed} - SFC_{Uninstalled}}{SFC_{Uninstalled}} \tag{2}$$

Where $Pu_{Installed}$ corresponds to the installed power, i.e., the power delivered by the engine installed on the helicopter, $Pu_{Uninstalled}$ corresponds to the

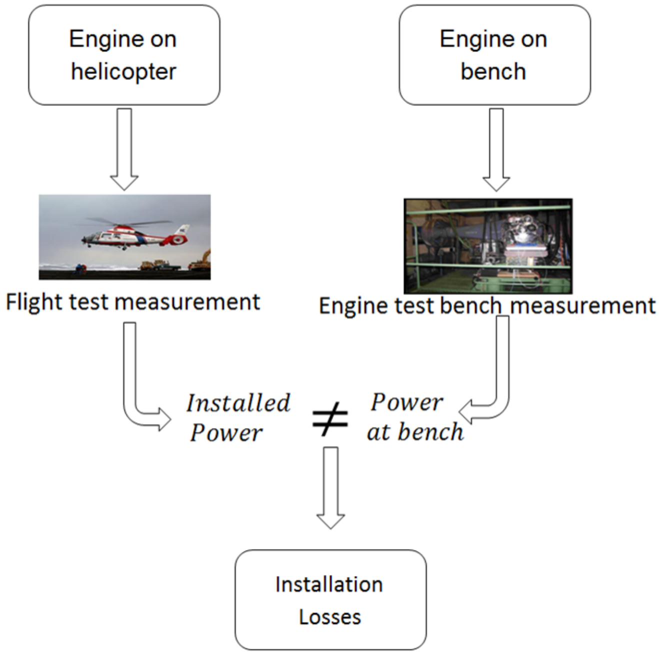

Figure 1: Installation effect definition

uninstalled power, i.e., the power delivered by the engine on the bench. The parameter $SFC_{Installed}$ corresponds to the specific fuel consumption installed, and $SFC_{Uninstalled}$ corresponds to the specific fuel consumption not installed.

Therefore, throughout this paper, when referring to the installation effect at a given N1 or ITT, which corresponds to the engine limit, the equation 1 will be used to calculate the installation effect and when referring to the installation effect at a given power, the equation 2 will be used.

2.2 System Loss definition

Helicopter engine installation effects are induced by aerothermal and aerodynamic disturbances generated by the installation of the engine on the helicopter. SAE 5642 Ref. 1 outlines the different sources of helicopter engine installation effects such as pressure drop, charge heating, pressure and temperature distortion, swirl induced by the air intake, and pressure drop induced by the exhaust system. This set of parameters will be referred as "System Loss" in the present paper.

Among these parameters, the air intake pressure drop (ΔP) stands out, primarily dictated by the air intake geometry. This drop is quantified as the disparity between external pressure and the mean pressure at the AIP.

Similarly impacting is the charge heating within the air intake (ΔT), attributed to compressibility effects inducing thermal elevation. Additionally, the position of the air intake on the helicopter can contribute to this charge heating through heat transfer from the engine compartment.

Pressure distortion, defined as pressure heterogeneity without altering the average pressure value at the AIP, is important. Based on insights from Kurzke Ref. 11, empirical evidence indicates a critical angle of approximately $60°$ for pressure distortion. Hence, in this study, we adopt the pressure distortion index defined as follows:

$$DC_{60} = \frac{P_{t60°,min} - P_{t,mean}}{\frac{1}{2}\rho V^2} \quad (3)$$

This equation allows us to quantify pressure distortion effectively within the analysis.

Temperature distortion, analogous to pressure distortion, albeit focusing on temperature field heterogeneity without altering its mean value. Despite being less explored than pressure distortion, limited studies, exist in the literature Ref. 12. AIR 5867 Ref. 13 introduces a method to quantify temperature distortion, considering the intensity of temperature field heterogeneity. Temperature distortion is described in the same way as pressure distortion with a critical angle of 120°.

$$TC_{120} = \frac{T_{120°,max} - T_{mean}}{T_{mean}} \quad (4)$$

Swirl, characterized by angular velocity at the AIP plane, is outlined in AIR 5686 Ref. 14, along with its impact on engine performance and operability. However, due to the challenges in measuring swirl during flight, it is not considered in this study.

The exhaust pressure drop, comprising diffusion disparities between helicopter and uninstalled exhaust, alongside static pressure differences at the ejector outlet, directly impacts power turbine output Ref. 15. While not a focus here, an empirical model of the pressure drop induced by the exhaust system is used in this study to show the capability of the method to predict the installation effect. However, a similar methodology will be used to create a surrogate model of the exhaust in future investigations.

2.3 Machine learning models and training process

2.3.1 Machine learning models

In this study, we evaluate the performance of various machine learning models in predicting aerodynamic criteria. The analysis focuses on regression models, which are suitable for predicting continuous outcomes. In this section, a simple explaination of all machine learning models tested during this study are performed.

We assessed the following machine learning models, all implemented in scikit-learn library Ref. 16:

- Linear Regression: Linear regression assumes a linear relationship between the input variables (predictors) and the output variable (response). It finds the best-fitting line that minimizes the sum of squared residuals (the vertical distance between each data point and the line). This model is simple yet effective for understanding the relationship between variables in a straightforward manner.

- Random Forest: Random Forest is an ensemble learning method that constructs many decision trees during training and outputs the mode of the classes (classification) or the average prediction (regression) of the individual trees. Each tree in the ensemble is built from a bootstrap sample of the training dataset and randomly selects a subset of features at each split point, providing robustness against overfitting and high predictive accuracy Ref. 17.

- Support Vector Regression (SVR): SVR is a type of support vector machine that is used for regression tasks. It works by mapping input variables into a high-dimensional feature space where it finds a hyperplane that best separates the output variable based on the input variables. SVR balances model complexity and prediction accuracy by using a regularization parameter that controls the width of the margin and a kernel function that specifies the mapping of the input variables into the feature space Ref. 18.

- Multi-Layer Perceptron (MLP) Regressor: MLP Regressor is a type of artificial neural network that uses multiple layers of nodes (neurons) to model complex relationships between inputs and outputs. Each neuron applies an activation function to the weighted sum of its inputs, allowing the network to capture nonlinear patterns in the data. Training an MLP involves adjusting the weights through backpropagation to minimize prediction errors, making it powerful for tasks where data relationships are not easily linearly separable Ref. 19.

- Gradient Boosting: Gradient Boosting is an ensemble technique where multiple weak learners (often decision trees) are built sequentially. Each subsequent model corrects the errors of its predecessor by focusing on the residuals (the difference between predicted and actual values). Gradient Boosting combines the predictions of these weak learners to produce a final strong learner with improved accuracy, using the strengths of each individual model to achieve high predictive performance Ref. 20.
- K-Nearest Neighbors (KNN): KNN is a non-parametric lazy learning algorithm used for both classification and regression tasks. It predicts the output variable based on the majority class (for classification) or the average of the closest k training examples in the feature space (for regression). KNN is simple to implement and understand, but its computational complexity grows with the size of the training dataset, making it less efficient for large datasets with many features Ref. 21.
- Bayesian Ridge Regression: Bayesian Ridge Regression is a probabilistic model that combines the principles of Bayesian inference with ridge regression. It assumes a prior distribution over the model parameters and updates this distribution based on the observed data to provide probabilistic predictions. This approach incorporates regularization, which helps prevent overfitting by penalizing large coefficients while maintaining flexibility in fitting the data Ref. 22.
- Lasso Regression: Lasso (Least Absolute Shrinkage and Selection Operator) Regression is a linear model that incorporates L1 regularization. It adds a penalty equal to the absolute value of the magnitude of coefficients to the loss function, promoting sparsity in the model by forcing insignificant coefficients to zero. Lasso regression is useful for feature selection in high-dimensional datasets where only a subset of the features have a major impact on the output variable Ref. 23.
- Ridge Regression: Ridge Regression is a linear regression model that incorporates L2 regularization. It adds a penalty equal to the square of the magnitude of coefficients to the loss function, which helps prevent overfitting by shrinking the coefficients. Ridge regression is particularly effective when there is multicollinearity (high correlation between predictor variables) in the dataset, as it reduces the influence of less important variables on the model's predictions Ref. 24.

2.3.2 Machine learning model training process

The machine learning model training process followed these steps:

1. Data Normalization: The dataset was normalized to ensure consistent scaling of all features, preventing any variable from disproportionately influencing the model.
2. Train-Test Split: The dataset was divided into train and test sets. The train set was used to train the model, while the test set was kept aside to evaluate its performance on unseen data.
3. Model Training: The model was trained using the training dataset to learn patterns and relationships between input features and the target variable.
4. 5-Fold Cross-Validation: To optimize model performance and ensure generalizability, a 5-fold cross-validation was employed. This involved splitting the training data into 5 subsets. The model was trained on 4 subsets and validated on the remaining subset. This process was repeated 5 times, with each subset used once as the validation data.
5. Grid Search for Hyperparameter Tuning: Grid search was performed to identify the optimal hyperparameters for the model. Hyperparameters such as regularization strength or number of trees in a random forest were systematically tested. Cross-validation performance metrics were used to evaluate each combination of

hyperparameters. The best combination was selected based on these metrics to maximize model performance on new, unseen data.

These steps ensured that the machine learning models were trained effectively, validated properly, and optimized to achieve the best possible performance on new, unseen data, minimizing any overfitting of the model.

2.4 Machine learning metrics

This paragraph introduces two commonly used metrics to compare and to assess the machine learning model performances, the coefficient of determination (R^2 score) and mean absolute error (MAE). The R^2 score, also known as the coefficient of determination, quantifies the proportion of the variance in the dependent variable that is predictable from the independent variables. It ranges from 0 to 1, with 1 indicating perfect prediction. Mathematically, it is calculated as:

$$R^2(y_i, \widehat{y_i}) = 1 - \frac{\sum_{i=1}^{n}(y_i - \widehat{y_i})^2}{\sum_{i=1}^{n}(y_i - \bar{y_i})^2} \quad (5)$$

Mean Absolute Error (MAE) measures the average magnitude of the errors in a set of predictions, without considering their direction. It is calculated as the average of the absolute differences between predicted and actual values:

$$MAE = \frac{1}{n}\sum_{i=1}^{n}|y_i - \hat{y}_i| \quad (6)$$

The MAE is in the same unit that the predicted variable, the lowest value being the better.

2.5 Surrogate model creation: Workflow

To introduce a new kind of air intake on an aircraft, two points need to be assessed:

- The air flow characteristics: each engine comes with air flow characteristics thresholds to respect, in order to ensure a nominal functioning of the engine. The respect of these criterion is demonstrated in flight. To proceed, a dedicated instrumentation is needed, like pressure and temperature racks in the air intake to measure the parameters described in 2.2. This instrumentation disturbs the flow which induces modifications of the installed performance.
- The installation effects: to assess the installation effects, a comparison is made between the in-flight measured performance and their equivalent on bench. The serial engine probes are used, without any additional disturbance of the air flow characteristics.

As the flights to demonstrate the compliance of the air flow characteristics remains essential, the proposed methodology intends to only use those flights to assess the installation effects via a new modeling method instead of direct measurement. The purpose is to make no more useful the flights dedicated to the installation effects measurement, reducing the flight test hours needed for the development of a new air intake.

The proposed methodology is made of two main steps:

- Build a surrogate model of the system loss of the targeted air intake (the new one)
  - Based on the system loss measurement during the flights for the air flow characterization. Those flights will be called ”air flow characterization flights”
  - Using machine learning regression models to learn measured parameters 2.2
- Apply the surrogate model on existing flight records of the source air intake (the initial one). Those flights will be called ”source flights”.

To proceed, an engine model is needed. The engine model will, on one hand, ingests the N1, ITT and power (and other contextual parameters) of the source flight to respectively produce the power at given N1, power at given ITT and SFC at given power needed to compute the installation effects. It will constitute the referential uninstalled set of performance. On the other hand, the model will ingest, additionally to the previous unchanged set of parameters, the outputs of the surrogate model of the system loss of the targeted air intake. Proceeding this way, the outputs of the engine model will be a set of installed parameters. The difference between the installed and the uninstalled sets of performance, according to eq 1 and eq 2, corresponds to the prediction of the installation effects of the targeted air intake. The complete workflow is schematized in figure 2.

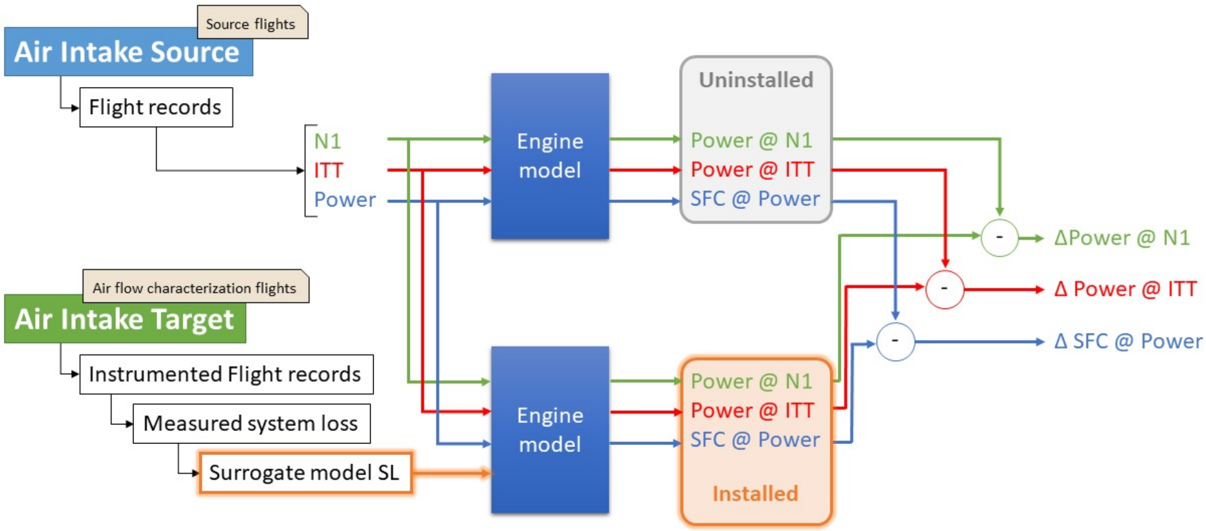

Figure 2: Installation effects prediction workflow

3 RESULTS & DISCUSSION

3.1 Air intake surrogate model

This section aims to assess the validity of the surrogate model used in this study. The initial database contains multiple flights and approximately 300 stabilized points. Before applying various machine learning models to build the surrogate model, we selected all the relevant variables by analyzing their correlations and checking the importance of each one. The retained variables include external aerodynamic characteristics, certain helicopter features, engine data, and specific features related to the filtered air intake.

3.1.1 Machine learning model selection

The table 1 presents the performance results of various machine learning models used to predict three aerodynamic criteria: DC60 (pressure distortion), DP (pressure drop), and TC120 (temperature distortion). The performance metrics include R^2 and MAE (mean absolute error). Below is a detailed analysis of the results.

For the DC60 parameter, the Gradient Boosting model stands out with an R^2 of 0.88 and a notably low MAE of 0.005. Given that the maximum value for DC60 is around 0.2 and an classical value is approximately 0.05, the MAE is 10 times lower than the classical value of pressure distortion. Other models like Random Forest, SVR, and KNN also show strong performance with R^2 values of 0.83 and MAEs around 0.0055, still well below the classical value.

For the DP parameter, Gradient Boosting and MLP Regressor again excel with R^2 values of 0.88 and MAEs of 0.23 and 0.25, respectively. Considering that DP values are generally around 1, these MAEs are approximately 4 times lower than the typical value.. The Random Forest model also performs well with an R^2 of 0.82 and an MAE of 0.32. SVR and KNN models show lower predictive power with R^2 values around 0.63.

Regarding the TC120 parameter, the Gradient Boosting model leads with an R^2 of 0.90 and an MAE of 0.00034. This MAE is pretty good as the maximum value for TC120 is around 0.02, and a typical value is about 0.005. This MAE is about 15 times lower than the typical value. The Random Forest model is a close second with an R^2 of 0.85 and an MAE of 0.00039. Other models like SVR and MLP Regressor show moderate performance, while linear models have the weakest performance with R^2 values below 0.58, and their MAEs are less competitive.

Overall, the Gradient Boosting model emerges as

Table 1: Performance metrics for various machine learning models predicting aerodynamic criteria.

Parameter	Model	R^2	MAE
DC60	Linear regression	0.72	7.4×10^{-3}
	Random forest	0.83	5.6×10^{-3}
	SVR	0.83	5.4×10^{-3}
	MLP regressor	0.78	7.0×10^{-3}
	Gradient Boosting	0.88	5.0×10^{-3}
	KNN	0.83	5.5×10^{-3}
	Bayesian Ridge	0.72	7.3×10^{-3}
	Lasso	0.72	7.4×10^{-3}
	Ridge	0.68	7.9×10^{-3}
DP	Linear regression	0.70	4.0×10^{-1}
	Random forest	0.82	3.2×10^{-1}
	SVR	0.63	4.2×10^{-1}
	MLP regressor	0.87	2.5×10^{-1}
	Gradient Boosting	0.88	2.3×10^{-1}
	KNN	0.64	4.2×10^{-1}
	Bayesian Ridge	0.70	4.0×10^{-1}
	Lasso	0.87	2.4×10^{-1}
	Ridge	0.80	2.7×10^{-1}
TC120	Linear regression	0.48	7×10^{-4}
	Random forest	0.85	3.9×10^{-4}
	SVR	0.68	6.2×10^{-4}
	MLP regressor	0.65	6.1×10^{-4}
	Gradient Boosting	0.90	3.4×10^{-4}
	KNN	0.53	7×10^{-4}
	Bayesian Ridge	0.57	6.7×10^{-4}
	Lasso	0.49	7.2×10^{-4}
	Ridge	0.53	7×10^{-4}

the best overall model for predicting all three criteria, with the highest R^2 values and the lowest MAE. Linear models (Linear Regression, Ridge, Lasso, and Bayesian Ridge) tend to underperform compared to non-linear models such as Random Forest, SVR, MLP, and Gradient Boosting. Based on this analysis, the Gradient Boosting model has been selected for creating the surrogate model in the subsequent sections of this paper. This choice is justified by its consistently superior performance across all three criteria.

3.1.2 Overfitting and Residual Analysis

In this section, we analyze the performance of the gradient boosting model in recalculating three aerodynamic criteria: TC120, DC60, and DP. We utilize the Mean Absolute Error (MAE) as the evaluation metric, plotting it against the number of iterations (n estimators) to visualize how the model's prediction accuracy evolves. They allow us to observe how quickly the model reduces errors on the training data and whether it converges to a stable solution. they can also help to detect overfitting by comparing train and test MAE curves.

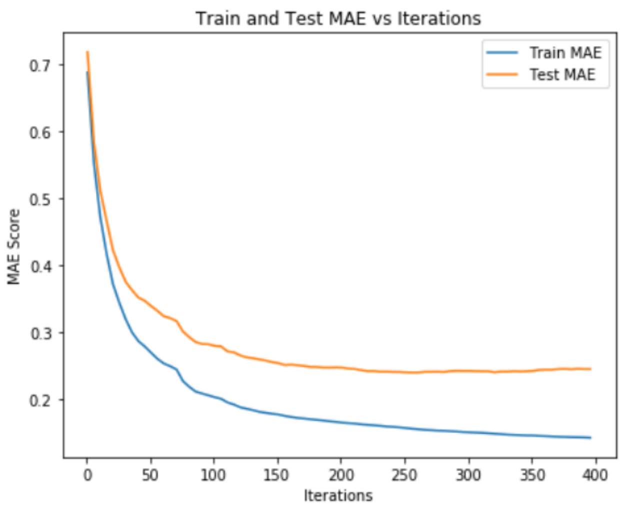

(a) Pressure drop prediction overfitting analysis

The pressure drop plot (figure 3a) shows a more gradual decline in both training and test MAE compared to the other two criteria. The training MAE steadily decreases over the first 200 iterations before leveling off, indicating continuous learning and improvement. The test MAE also decreases initially but starts to level off around 150 iterations and stabilizes at a higher value than the training MAE. This suggests that the model improves its predictions on both training and test data, but there remains a consistent gap between the two, indicating some degree of overfitting.

For the DC60 criterion (figure 3b), the training MAE decreases dramatically within the first 50 iterations, after which it flattens, indicating that the model quickly reaches a low error rate on the training data. The test MAE also shows a steep decline initially but then stabilizes at a higher value compared to the training MAE, suggesting a potential overfitting issue. The gap between the training and test MAE after the initial iterations indicates that while the model performs very well on the training data, its performance on unseen data is slightly worse, pointing to an overfitting tendency.

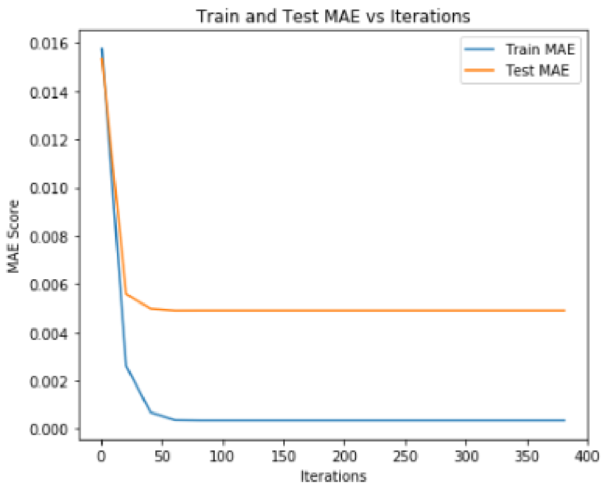

(b) Pressure distortion overfitting analysis

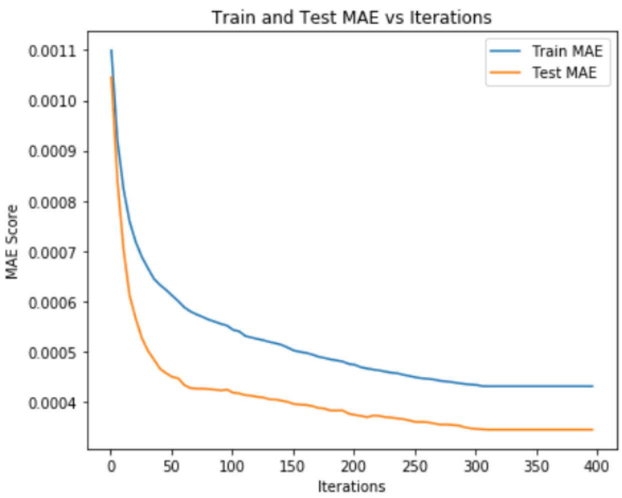

(c) Temperature distortion overfitting analysis

Figure 3: Gradient boosting model: overfitting analysis

In the TC120 plot (figure 3c) , the training MAE starts relatively high and decreases significantly over the first 100 iterations, showing a rapid improvement in model performance. Beyond 100 iterations, the decrease in training MAE becomes more gradual, indicating the model is fine-tuning its predictions. The test MAE follows a similar pattern, initially decreasing rapidly and then stabilizing, but it consistently stays below the training MAE after around 50 iterations. This suggests that the model generalizes well to the test data without overfitting.

To evaluate the performance of the machine learning models, we analyzed the residuals using Q-Q (Quantile-Quantile) plots. The Q-Q plots compare the quantiles of the residuals to the quantiles of a theoretical normal distribution. If the points follow the red line, it indicates that the residuals are normally distributed. Deviation from this line suggests potential issues with the model.

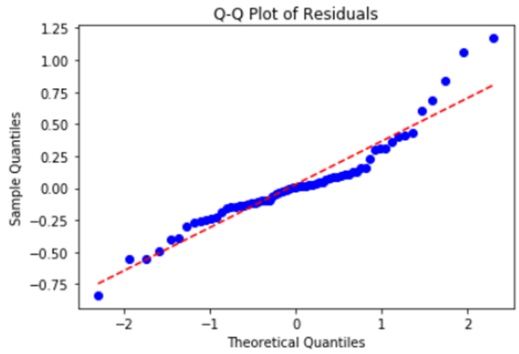

Figure 4: Q-Q Plot of Residuals for pressure drop gradient boosting model

The Q-Q plot of residuals for Model DP shows a slight deviation from the red line at both the lower and upper ends. This suggests that the residuals do not perfectly follow a normal distribution, especially for extreme values. This could indicate the presence of outliers or underfitting of the data at the extremes.

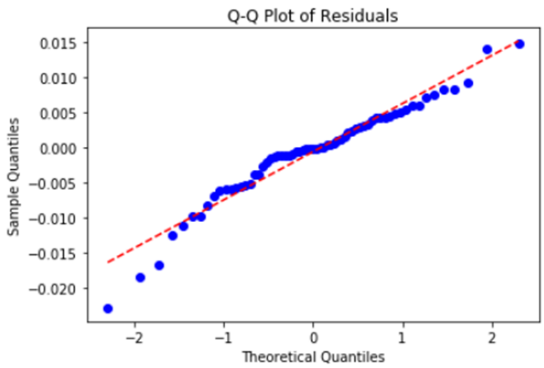

Figure 5: Q-Q Plot of Residuals for pressure distortion gradient boosting model

The Q-Q plot of residuals for Model DC60 presents better conformity to the red line compared to Model DP. However, slight deviations are still observed at the extremities, though they are less pronounced. This indicates that while the residuals are closer to a normal distribution, there are still areas where the model could be improved.

The Q-Q plot of residuals for Model TC120 shows very good agreement with the red line, suggesting that the residuals follow a normal distribution. The

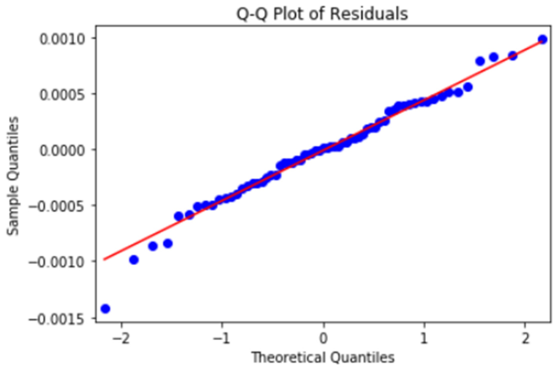

Figure 6: Q-Q Plot of Residuals for temperature distortion gradient boosting model

deviations at the extremities are minimal, indicating that this model captures the characteristics of the data well and produces well-distributed residuals.

These results indicate that the models are well-generalized except for pressure distortion which has a risk of slight overfitting, however Q-Q plots don't point overfitting for pressure distortion. in conclusion, the analysis shows that Gradient Boosting is a suitable choice for developing surrogate models for predicting the aerodynamic criteria. The convergence points and the steady performance of the test MAE confirm that the models are robust and reliable for practical applications.

3.1.3 Surrogate model validation

This section aims to compare results from the surrogate model with real flight test data to assess its suitability for predicting installation effects. It analyzes three aerodynamic criteria by examining the errors made and their impact on installation effect predictions. Finally, a comparison with actual inlet data from other previously unlearned flights verifies the accuracy of the aerodynamic criteria predictions.

Pressure drop

Figure 7 illustrates the deviation between the surrogate model's predictions and the measured values from the test dataset. In Figure 7a, the predicted pressure drop values are plotted against the theoretical values. It is observed that the predictions remain within a $\pm 20\%$ relative deviation range of the pressure drop value. To assess the impact of this error on the installation effect prediction, we analyze the distribution of the absolute deviation between the predicted and theoretical values (see Figure 7b). The results show that 95% of the prediction errors lie between -0.5% and $+0.5\%$, with a mean absolute error of approximately 0.2%. This corresponds to a model-generated dispersion of about 0.4% on the installation effect, which is low given the other sources of uncertainty. Therefore, the surrogate model's accuracy is deemed sufficient.

A further validation step ensures that the model accounts for the specific characteristics of the filtered air intake. the surrogate model is applied to test

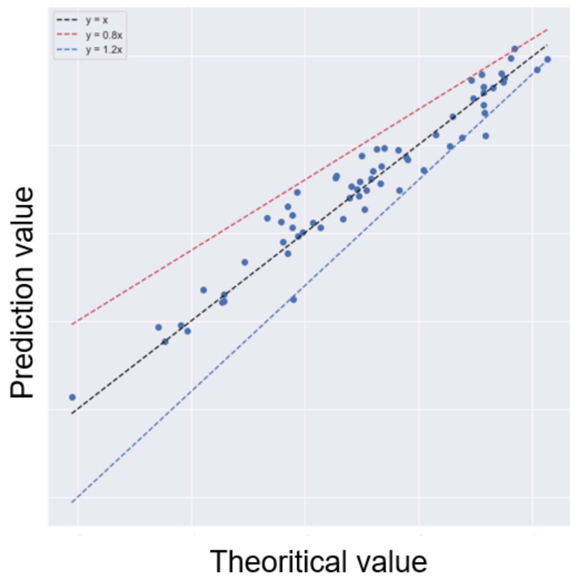

(a) Pressure drop prediction accuracy

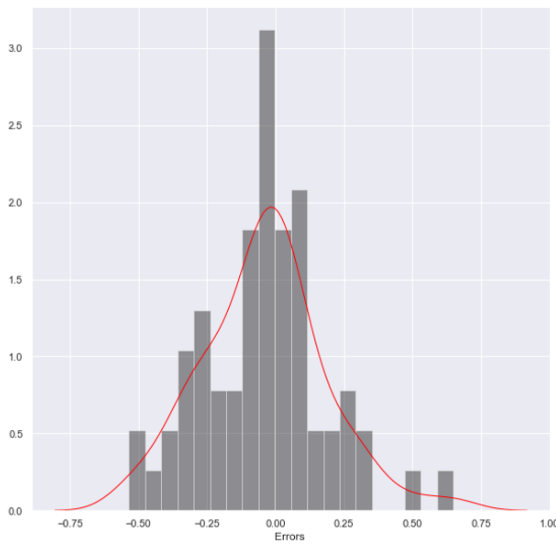

(b) Pressure drop deviation distribution

Figure 7: Comparison of pressure drop prediction accuracy and deviation distribution.

points from the installation effects campaign in a non-filter configuration, recalculating the pressure drop for each point assuming a configuration change to a filtered air intake. These recalculated values were then compared with actual tests in the filtered configuration. Figure 8 plots the pressure drop against the true airspeed (TAS), with the green points representing the surrogate model predictions and the blue points representing flight test results in the filtered configuration. The predicted values align well with the flight tests. An evolution corresponding to the helicopter's speed is clearly visible, linked to the formula involving the squared speed of the flow. Additionally, two distinct rows of points are observed for the same helicopter speed, indicating varying pressure drops. These variations correspond to the position of the filtered air intake by-pass. In fact, one of the characteristics of the filtered air intake is that it is necessary to have a by-pass in order to be able to open the by-pass in case of a excessive clogging of the filter, thus maintaining the air supply to the engine. It is evident that the surrogate model takes the bypass into account for the prediction. The pressure drop generated by the filtered air intake is accurately predicted by the surrogate model.

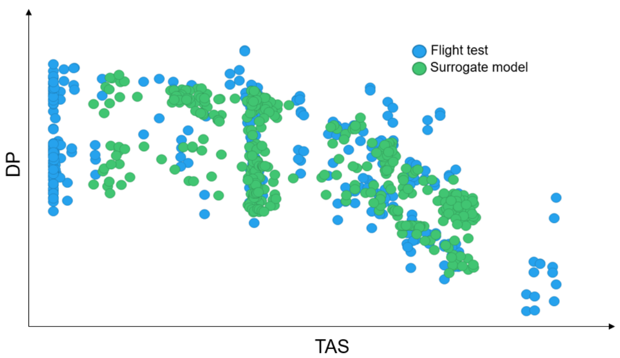

Figure 8: Pressure drop prediction of the surrogate model validation by comparison with flight test result for IBF config using gradient Boosting based model

Pressure distortion (DC60)

Thereafter, the same analysis is performed for the pressure distortion. We can see from the figure that most of the points are within 20% of the measured value of the pressure distortion. However, some points are still overestimated relative to this 20% deviation. If we look at figure 9, we notice that most of the time the error is included between 0.0075 which corresponds to an uncertainty generated by the model on the installation effect of the order of $\pm 0.1\%$ at constant ITT, which is sufficient. However, a much larger deviation up to 0.02 can generate a maximum uncertainty of $\pm 0.25\%$ at constant ITT. We consider the model to be valid for the prediction of the pressure distortion.

The second step of validation consists of the use of a surrogate model on test points resulting from the installation effect campaign in non-filtered air intake,

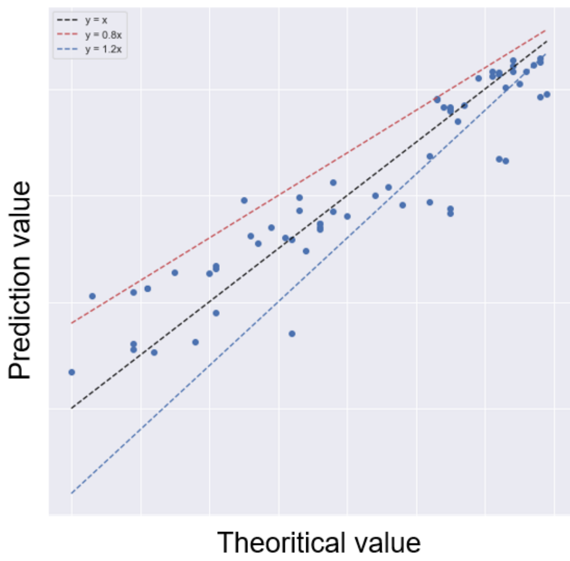

(a) Pressure distortion prediction accuracy

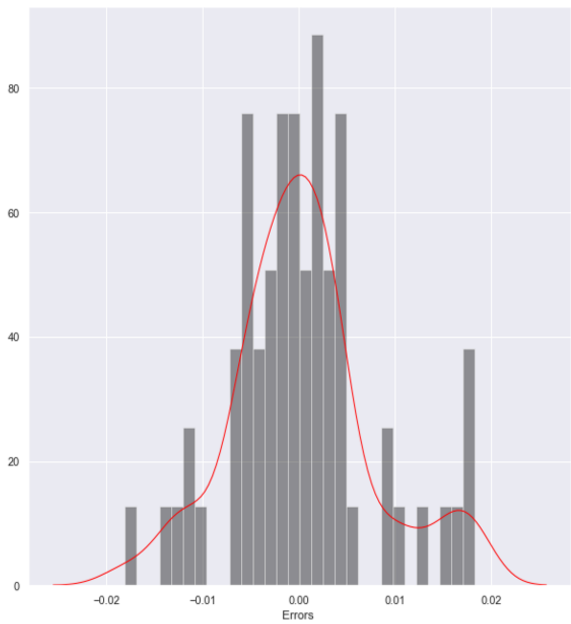

(b) Pressure distortion deviation distribution

Figure 9: Comparison of pressure distortion prediction accuracy and deviation distribution.

and we recalculated the pressure distortion associated with each point in the case that the configuration changed, i.e., that these same flight points were performed with a filtered air intake. Afterwards, we compared the measurements with real flight test measurements in filtered configuration. The figure 10 plots the pressure distortion according to the TAS, the green points correspond to the pressure distortion predicted by the surrogate model and the blue points to the point resulting from flight tests in filtered configuration. To begin the analysis, we can see that the DC60 seems to be well predicted compared to the flight tests. We can also observe several things. Indeed, in the case of the DC60 with filtered air intake, we notice that it does not depend on the TAS. Moreover, we can separate the graph into two parts, the upper part, where the DC60 corresponds to the left air intake, and the bottom than which corresponds to the right air intake. We also notice on each side a separation of the values, which corresponds to the opening and closing states of the bypass. Taking into account the accuracy of the measurement in flight, we consider that the surrogate model well represents the filtered air intake in the different flight phases and can thus be used to find the associated values of DC60.

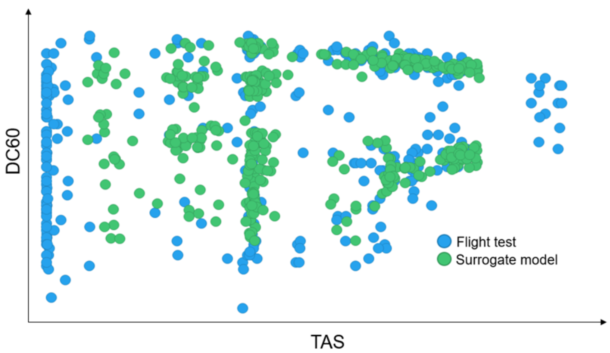

Figure 10: Pressure distortion prediction of the surrogate model validation by comparison with flight test result for IBF config using gradient Boosting based model

Temperature distortion (TC120)

The last parameter calculated by the surrogate model of the system loss is the temperature distortion. As for the pressure distortion and the pressure drop generated by the air intake, an analysis of the accuracy of the prediction is carried out, followed by a comparison with the flight tests as well as an analysis of the influence parameters. The figure 11a illustrates the deviation between the predicted value and the theoretical value. We notice that most of the points are included between the red line and the blue line, which corresponds to a relative deviation of 20% on the predicted value. If we examine the deviation, the figure 11b represents the distribution of the error committed in relation to the measured temperature distortion. We can see that 95% of the error is between 0.001 and -0.001 which corresponds to an impact on the installation effect of about $\pm 0.15\%$. Therefore, we

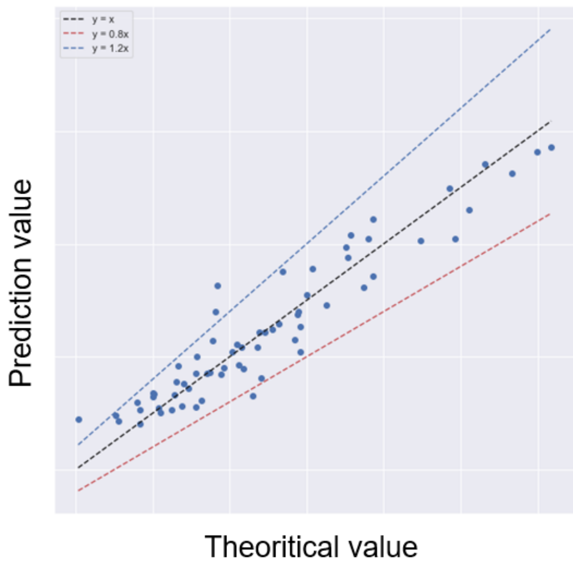

(a) Temperature distortion prediction accuracy

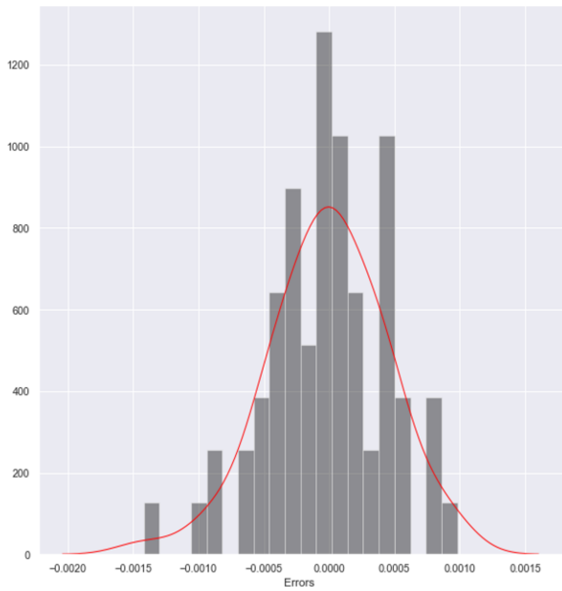

(b) Temperature distortion deviation distribution

Figure 11: Comparison of temperature distortion prediction accuracy and deviation distribution.

consider the accuracy of the prediction sufficient.

The next step for the validation of the surrogate model is to compare it with the flight tests. The figure 12 presents the evolution of the TC120 with the TAS and allows to compare the prediction from the surrogate model with the flight tests. We can see that the prediction seems to fit well with the flight test values.

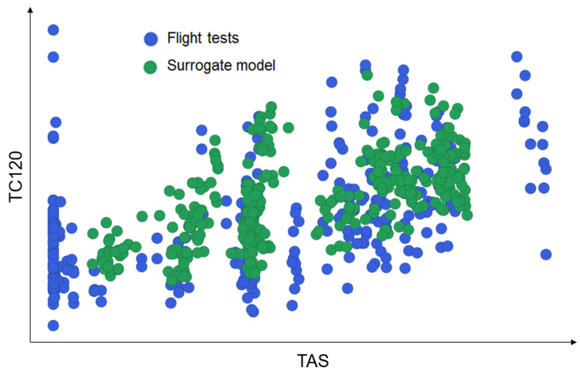

Figure 12: Temperature distortion prediction of the surrogate model validation by comparison with flight test result for IBF config using gradient Boosting based model

3.2 Installation effect prediction

This part aims to validate the method proposed in the part 2.5 for the prediction of installation effects. For this purpose, the installation effects of a filtered configuration are calculated using the surrogate model previously created and applied on flight points from a real non-filtered air intake installation effects campaign. Then a thermodynamic model is used to assess the impact of this system loss on the engine and therefore the installation effect. Firstly, for each point of the installation effects campaign in non-filtered air intake, a system loss associated to the filtered air intake is generated. Moreover, in order to be able to compare the installation effects measured in flight, the impact of the nozzle on the installation effects is taken into account with the theoretical pressure drop generated by the nozzle. Afterwards, for each point, the power delivered by the engine is calculated using the thermodynamic engine model created in Ref. 2 and the filtered air intake system loss. Finally, using the thermodynamic engine model, the same points are simulated without system loss in order to calculate the uninstalled power and so the installation effects.

The figure 13a plots the installation effects as a function of the corrected power at N1 fixed. The green points correspond to the installation effects calculated using the method explained in this paper. The blue points correspond to the installation effects obtained from an installation effect campaign with a filtered air intake in order to validate the method. The light colors correspond the the open bypass door configuration, while dark colors correspond to the closed bypass door configuration. We notice that the installation effects are well predicted by the method proposed in this chapter. Indeed, we observe the effect of the installation side of the engine as well as the impact of the opening and closing of the bypass. Moreover, we can see that the light blue and light green points are well superposed, as well as the dark points. However, we notice that some points, where the installation effects are important (large negative values), are at the bottom of the scatter plot. This can be explained by the fact that these points may be subject to errors on the torque measurement. Furthermore, the shape seems to be well captured by the model.

Figure 13b shows the installation effects as a function of the corrected power at a given ITT. In this case, we also observe a good prediction of the installation effects, with a slight overestimation of less than 1% between the installation effects calculated in the case of the closed bypass and the installation effects resulting from the flight tests in the case of the closed bypass. Moreover, the shape of the installation effect seems to be well captured by the model.

To conclude, the figure 13c shows the impact of the installation of the engine on the consumption at a given power as a function of the corrected power. It can be seen that, once again, the installation effects are well predicted. Nevertheless, some deviation can be observed that can be explained by the accuracy of the fuel flow measurement sensor, which is subject to strong uncertainties. Indeed, by looking at the values of these extreme points, it is highly probable that these points are outliers. Concerning the shape of the installation effects, they are well represented.

4 CONCLUSION

In conclusion, this paper introduces an advanced machine learning method for predicting installation effects on air intake configurations, offering enough accuracy to reduce the number of flight tests during de-

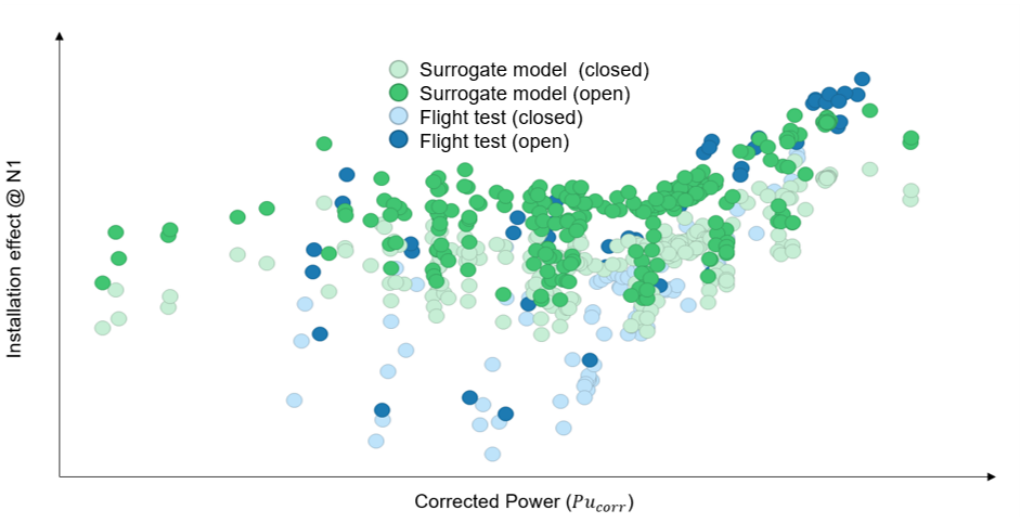

(a) Installation effect prediction with air intake surrogate model at given N1

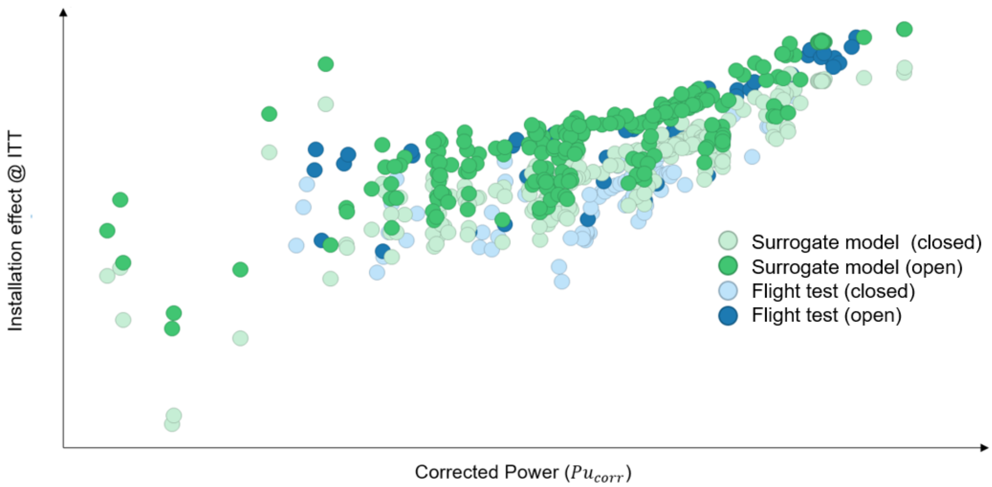

(b) Installation effect prediction with air intake surrogate model at given ITT

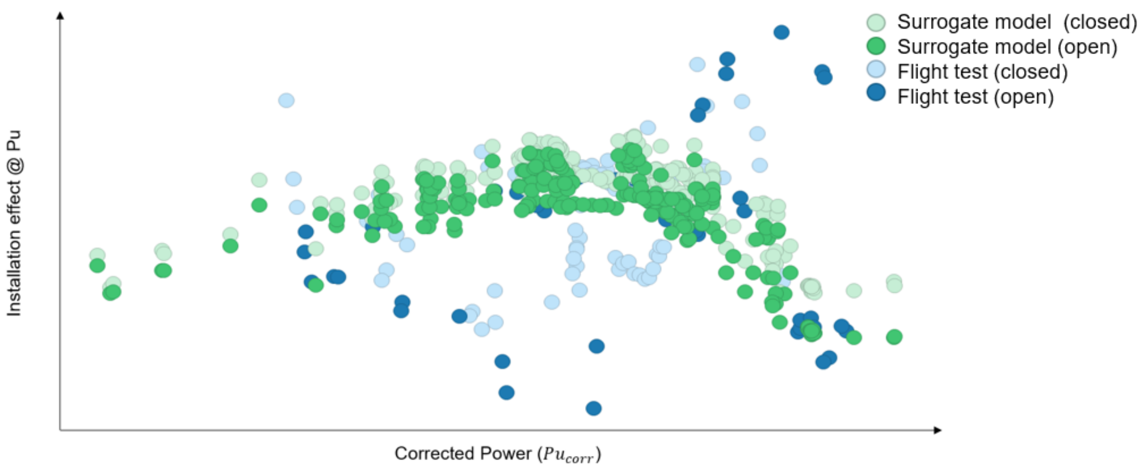

(c) Installation effect prediction with air intake surrogate model at given Pu

Figure 13: Installation effect prediction with air intake surrogate model under different conditions: (a) at given N1, (b) at given ITT, (c) at given Pu.

velopment. The key findings of this methods are:

- Evaluation of several machine learning models, with Non-linear models that outperform linear models in predicting aerodynamic criteria (DC60, DP, TC120). Especially, the Gradient Boosting model consistently demonstrates the best performance with the highest R^2 and the lowest MAE across all criteria.
- The overfitting analysis shows that the Gradient Boosting model effectively learns the patterns in the data for DP, DC60, and TC120 without overfitting, as evidenced by the convergence of the test MAE and the continuous decrease of the training MAE, indicating robust generalization capabilities. The Q-Q plots reveal that while the residuals for DP shows some deviation from normality, DC60 and TC120 exhibit better conformity, indicating well-distributed residuals and confirming the reliability of the models.
- Surrogate model validation shows good performances in predicting aerodynamic and aerothermal criteria
  - The surrogate model for pressure drop accurately predicts values within a ±20% relative deviation range, with 95% of errors between -0.5% and +0.5%, demonstrating sufficient accuracy and minimal impact from other uncertainties. Validation against flight test data confirms the model's reliability in predicting pressure drops.
  - The surrogate model for pressure distortion predictions generally falls within a 20% deviation from measured values, with most errors within ±0.1% leading to an estimation of ±0.25% on the installation effect prediction. Comparison with flight test data shows good agreement.
  - The surrogate model for temperature distortion maintains a high level of accuracy, with 95% of errors within ±0.001, corresponding to an installation effect impact on installation effect prediction of about ±0.15%. Validation against flight test results shows the model's predictions align well with actual measurements.
- Installation effect prediction with the workflow proposed is well predicted, the shapes of the installation effects are well reproduced and the maximum estimated error is of the order of 1% a given ITT, less at given power and given N1. This accuracy is sufficient for estimating installation effects.

To conclude, this study opens up new perspectives by easing the development of new air intake configurations and exploring the use of reduced-order models. These models could enable rapid computation of aerodynamic criteria in flight, faster than traditional CFD simulations, making it possible to estimate installation effects under different flight conditions. This approach could enable installation effects to be computed continuously during flight. In addition, this approach could pave the way for the creation of a digital twin for air intakes, enabling proactive detection of anomalies.

Author contact

Alexandre DI-MARCO,
alexandre.di-marco@airbus.com
Florent ESTERLE, florent.esterle@airbus.com
François-Xavier GAULMIN,
francois.gaulmin@airbus.com@airbus.com

References

[1] SAE, "The effect of installation power losses on the overall performance of a helicopter," *TechnicalReport AIR 5642*, 2005.

[2] A. Di-Marco, C. Lecauchois, B. Fayard, and P. Sagaut, "A predictive method for helicopters engine installation losses determination," in *Proceedings of the ASME Turbo Expo 2022: Turbomachinery Technical Conference and Exposition. Volume 1: Aircraft Engine; Ceramics and Ceramic Composites.*, ser. Turbo Expo: Power for Land, Sea, and Air, Jun. 2022. DOI: 10.1115/GT2022-82243. [Online]. Available: https://doi.org/10.1115/GT2022-82243.

[3] A. Di-Marco, C. Lecauchois, B. Fayard, and P. Sagaut, “Helicopters engine integration: From CFD deep airflow analysis to general impact on helicopter engine performance,” in *AIAA AVIATION 2022 Forum*, 2022. DOI: 10.2514/6.2022-3687.

[4] M. Migliorini, P. K. Zachos, D. G. MacManus, and P. Haladuda, “S-duct flow distortion with non-uniform inlet conditions,” *Proceedings of the Institution of Mechanical Engineers, Part G: Journal of Aerospace Engineering*, vol. 237, no. 2, pp. 357–373, 2023.

[5] A. Di-Marco, J. Jacob, and P. Sagaut, “Unsteady characteristics of pressure and swirl distortion in helicopter intake: A lattice boltzmann method approach,” *Aerospace Science and Technology*, vol. 138, p. 108 333, 2023.

[6] S. L. Brunton, J. Nathan Kutz, K. Manohar, *et al.*, “Data-driven aerospace engineering: Reframing the industry with machine learning,” *AIAA Journal*, vol. 59, no. 8, pp. 2820–2847, 2021.

[7] M. Aliramezani, C. R. Koch, and M. Shahbakhti, “Modeling, diagnostics, optimization, and control of internal combustion engines via modern machine learning techniques: A review and future directions,” *Progress in Energy and Combustion Science*, vol. 88, p. 100 967, 2022.

[8] S. Le Clainche, E. Ferrer, S. Gibson, E. Cross, A. Parente, and R. Vinuesa, “Improving aircraft performance using machine learning: A review,” *Aerospace Science and Technology*, vol. 138, p. 108 354, 2023.

[9] J. Kou and W. Zhang, “Data-driven modeling for unsteady aerodynamics and aeroelasticity,” *Progress in Aerospace Sciences*, vol. 125, p. 100 725, 2021.

[10] J. Nagawkar and L. Leifsson, “Multifidelity aerodynamic flow field prediction using random forest-based machine learning,” *Aerospace Science and Technology*, vol. 123, p. 107 449, 2022.

[11] J. Kurzke and I. Halliwell, “Inlet flow distortion,” in *Propulsion and Power: An Exploration of Gas Turbine Performance Modeling*. Springer International Publishing, 2018, pp. 249–267. DOI: 10.1007/978-3-319-75979-1_6.

[12] W. BRAITHWAITE, J. E. GRABER, and C. MEHALIC, “The effect of inlet temperature and pressure distortion on turbojet performance,” in *9th Propulsion Conference*. DOI: 10.2514/6.1973-1316.

[13] SAE, “Assessment of the inlet/engine total temperature distortion problem,” *TechnicalReport AIR 5867*, 2010.

[14] SAE, “Methodology for assessing inlet swirl distortion,” *TechnicalReport AIR 5686*, 2010.

[15] *The Predicted and Measured Effects of Increasing Back Pressure on the Performance of a Turboshaft Engine*, vol. Volume 1: Aircraft Engine; Ceramics; Coal, Biomass and Alternative Fuels; Education; Electric Power; Manufacturing Materials and Metallurgy, Turbo Expo: Power for Land, Sea, and Air, Jun. 2010, pp. 79–88. DOI: 10.1115/GT2010-22323.

[16] F. Pedregosa, G. Varoquaux, A. Gramfort, *et al.*, “Scikit-learn: Machine learning in python,” *Journal of Machine Learning Research*, vol. 12, pp. 2825–2830, 2011.

[17] L. Breiman, “Random forests,” *Machine Learning*, vol. 45, no. 1, pp. 5–32, 2001.

[18] A. J. Smola and B. Schölkopf, “A tutorial on support vector regression,” *Statistics and Computing*, vol. 14, no. 3, pp. 199–222, 2004.

[19] R. Hecht-Nielsen, “Artificial neural networks: A tutorial,” *Computers & Operations Research*, vol. 13, no. 2-3, pp. 116–124, 1990.

[20] J. H. Friedman, “Greedy function approximation: A gradient boosting machine,” *Annals of Statistics*, vol. 29, no. 5, pp. 1189–1232, 2001.

[21] T. M. Cover and P. E. Hart, “Cover, t. m., & hart, p. e. (1967). nearest neighbor pattern classification,” *IEEE Transactions on Information Theory*, vol. 13, no. 1, pp. 21–27, 1967.

[22] T. Park and G. Casella, “Bayesian regression modeling with the Lasso,” *Journal of the American Statistical Association*, vol. 103, no. 482, pp. 681–686, 2008.

[23] R. Tibshirani, “Regression shrinkage and selection via the lasso,” *Journal of the Royal Statistical Society. Series B (Methodological)*, vol. 58, no. 1, pp. 267–288, 1996.

[24] A. N. Tikhonov and V. Y. Arsenin, “The treatment of inverse problems by bayesian inference,” *Soviet Mathematics Doklady*, vol. 5, no. 3, pp. 1031–1035, 1977.